# Focused Ion Beam Fabrication: Process Development and Optimization Strategy for Optical Applications

**Vivek Garg, Rakesh G. Mote and Jing Fu**

**Abstract** This work presents an optimization of focused ion beam (FIB) milling process for the fabrication of optical elements. Focused ion beam is a nanofabrication tool involving ion–beam material interaction at atomic or molecular levels. The ion–solid interactions have been investigated for the fabrication of desired 3D geometries. Focused ion beam dwell time is an important parameter and determines the final geometry and accuracy of the fabrication. An algorithm has been developed to optimize the ion beam dwell time for the desired geometry fabrication maintaining high accuracy. Binary Fresnel zone plates (FZPs) have been fabricated using the optimized simulation results for demonstration. The algorithm can be used for fabrication of 3D elements and micro/nano-structures for various applications.

**Keywords** Focused ion beam · Nanofabrication · Optimization and simulation Micro/nano-optical elements

**Nomenclature**

| | |
|---|---|
| $a_{ij}$ | Milling coefficient |
| $A$ | Matrix to measure the milling coefficients |
| $F(t)$ | Objective function |
| $f$ | Focal distance |
| $G(x)$ | Standard normal Gaussian distribution |
| $I_B$ | Ion beam current |

V. Garg
IITB Monash Research Academy, Mumbai 400076, India
e-mail: vivekgarg@iitb.ac.in

R. G. Mote (✉)
Department of Mechanical Engineering, Indian Institute of Technology Bombay, Mumbai 400076, India
e-mail: rakesh.mote@iitb.ac.in

J. Fu
Department of Mechanical and Aerospace Engineering, Monash University, Clayton 3800, Australia
e-mail: jing.fu@monash.edu

© Springer Nature Singapore Pte Ltd. 2018

S. S. Pande and U. S. Dixit (eds.), *Precision Product-Process Design and Optimization*, Lecture Notes on Multidisciplinary Industrial Engineering,
https://doi.org/10.1007/978-981-10-8767-7_8

| | |
|---|---|
| $M$ | Number of pixels to be machined |
| $N$ | Total number of pixels |
| $p$, $Q$, $r$ | Multiplication matrices |
| $R$ | Radius |
| $t$ | Ion beam dwell time |
| $t^0$ | Initial value of dwell time |
| $t^k$ | Dwell time from $k$th update |
| $T$ | Ion beam milling time |
| d$x$, d$y$, d$z$ | Milled dimensions (length, width, depth) |
| $Y_s$ | Erosion rate |
| $z^o$ | Desired geometry profile |
| $\lambda$ | Wavelength |
| $\mu$ | Mean value |
| $\sigma$ | Standard deviation |
| $\Delta r_{\mathrm{Rayleigh}}$ | Rayleigh resolution limit |

## 1 Introduction

Focused ion beam (FIB) is an important and advanced technology in the field of micro/nano-fabrication. It has wide range of capabilities from milling and deposition to imaging at micro/nano-scale. The distinct advantage of FIB lies in the fact that it enables mask-less direct fabrication on various materials, making it suitable for applications in the field of nanotechnology. Focused ion beam instrument, when combined with imaging technologies like scanning electron microscope (SEM), offers a wide range of applications for fabrication and characterization of micro/nano-structures. It allows mask-less and one-step fabrication, which makes it a very important technology in micro/nano-fabrication. This is because the FIB milling does not require any intermediate resist layer as in other photo or e-beam lithographic techniques, and thus enables direct writing of micro/nano-structures. Focused ion beam has a short wavelength with high energy density, which helps focusing the beam to a smaller spot size of 5–10 nanometre (nm). It allows control of beam shape and size for fabrication of complex 3D structures. The unique fabrication capabilities of FIB make it an excellent tool for rapid prototyping applications. A great detail of research exists in the literature for FIB principle, its applications and limitations (Melngailis 1987; Lehrer et al. 2001; Reyntjens and Puers 2001; Kim et al. 2012; Mote and Xiaomin 2017). Focused ion beam processing has also been applied for processing and characterization of biological, organic materials, etc. (Fu and Joshi 2010; Al-Abboodi et al. 2013; Adineh et al. 2015), allowing its use for multidisciplinary research.

Focused ion beam is a specialized process and involves several complexities in terms of beam control and fabrication accuracy. Accurate FIB fabrication of optical

elements and 3D micro/nano-structures for specific applications require deep insight into the process. The accuracy of FIB fabricated profiles depends on a number of parameters such as scanning strategy, beam current, acceleration voltage, beam dwell time, etc. Out of these parameters, ion beam dwell time is one of the important parameters that determine the final geometry and accuracy of fabricated structures. A better understanding of the milling mechanisms and material removal at micro/nano-level is required for accurate fabrication and desirable performance of these elements. This will allow accurate fabrication of optical elements or any other 3D structure for specific applications in X-ray optics, micro/nano-photonics, etc.

In the present work, an optimization problem is formulated for FIB fabrication and has been solved in MATLAB by an iterative approach for an optimal solution. The algorithm minimizes the deviation of a simulated geometry obtained by FIB fabrication from the desired geometry. The proposed strategy can be further used to fabricate optical elements or any 3D micro/nano-structures. The ion beam dwell time has been optimized for the desired geometry fabrication, maintaining the required accuracy. This algorithm has been used to demonstrate the simulation of Fresnel zone plate (FZP) for specific design. Experiments have been carried out to validate the optimization model. Based on the optimization results, the designed FZP has been successfully fabricated.

The remaining chapter is organized in the following way. Focused ion beam micro/nanofabrication basics, process capabilities and limitations along with important FIB operating parameters and their effects have been discussed and assessed critically in Sect. 2. Section 3 presents the formulation of optimization problem and iterative solution approach for FIB nanofabrication. Simulation results have been illustrated in Sect. 4. Focused ion beam experiments and results have been included in Sect. 5. Finally, a conclusion and outlook are discussed in Sect. 6.

## 2 Focused Ion Beam Nanofabrication—Basics

The focused ion beam technique utilizes a finely focused beam of ions for milling, imaging, deposition, implantation, etc. A high-energy ionized beam of ions in a FIB system is produced from a liquid metal ion source (LMIS) by the application of electric field. This beam is focused onto a target surface, which results in a number of phenomena such as sputtering of constituent atoms, generation of collision cascade, surface modification, etc. Heavy ions also produce secondary electrons from the target surface, which can be used for imaging applications. Focused ion beam can also be used for deposition, implantation and lithography applications. In this section, FIB instrument, basic principle, ion–solid interactions and important parameters for FIB fabrication are discussed.

## 2.1 Focused Ion Beam Instrument

A typical dual beam FIB-SEM instrument has a liquid metal ion source (LMIS), an ion column, an electron column, a stage, detectors, a gas injection system (GIS), a vacuum system and a computer. An illustration of a Carl Zeiss Auriga dual beam FIB-SEM system (Compact-4558) available at IIT Bombay is shown in Fig. 1a.

The focused ion beam system is similar to a scanning electron microscope, where an electron beam is used. Both the systems employ charged particles, which can be used for imaging, etching and deposition applications. Use of ions in FIB offers several advantages over the electrons, due to the reason that ions are comparatively massive and larger. Ions have much more direct effect on the sample as compared to electrons, whereas electrons penetrate deeper due to their smaller size. Energetic ions carry higher momentum than electrons, which is used for material removal and milling applications. Another difference between the two systems lies in the beam steering and focusing optics. In SEM, magnetic fields are used to focus the electron beam due to smaller mass of electrons. On the other hand, charged ion beam requires stronger field; hence, electrostatic lenses are used. In a dual beam system, FIB and SEM columns are arranged at an angle of 52° to each other, which allows milling/deposition/etching by FIB and simultaneous observation through SEM. The sample is made normal to FIB by tilting the sample stage at 52°. A typical configuration of FIB-SEM columns and sample inside the vacuum chamber in a dual beam system is shown in Fig. 1b.

A highly focused ion beam is obtained from LMIS, which has a tungsten needle. The tungsten (*W*) needle is attached to a reservoir of source material. Gallium (Ga) is most commonly used FIB source because of the following reasons:

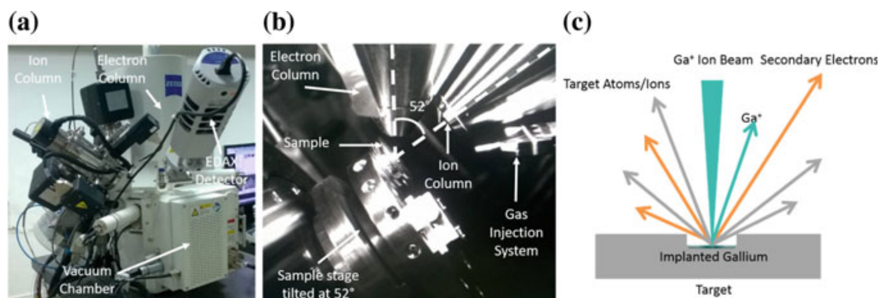


**Fig. 1** Focused ion beam (FIB) system at IIT Bombay: **a** Carl Zeiss Auriga Compact-4558 FIB-SEM system, **b** the dual beam-sample configuration inside vacuum chamber and **c** schematic illustration of FIB interaction with target material: sputtering of target atoms/ions, Ga ion implantation and generation of secondary electrons from target surface

- Low melting point (29.8 °C)—It requires less heating and avoids any interaction of Ga with tungsten needle.
- Low vapour pressure—It can be used in pure form and promotes long life, avoiding the Ga evaporation.
- Gallium has suitable mechanical, electrical and vacuum properties. Gallium emission provides high angular intensity with a small spread of energy.
- Low volatility at melting point—long source life.

The heated LMIS flows and wets the tungsten needle, having a tip radius of 2–5 μm. Gallium requires less reheating and remains liquid at ambient conditions for weeks due to its supercooling properties. If an electric field ($10^8$ V/cm) is applied at the end of wet tungsten needle, it will cause Ga to form a point source (2–5 nm) of conical shape (Taylor cone). This shape is formed as a result of balance between surface tension of the liquid metal and the electrostatic force set up by the applied electric field. Once the cone tip is formed and is sharp enough, the extraction voltage pulls Ga ions from the tungsten tip by ionization process. The Ga ions are then passed through the ion column, where an acceleration voltage (5–50 kV) is applied. A set of apertures and lenses are used in the ion beam column to focus the ion beam of various diameters at target surface. The spot size (diameter) and the shape of the beam govern its machining and imaging capabilities.

### *2.2 Ion–Solid Interactions*

The incident ion beam loses its energy to target electrons and atoms, when scanned over the sample surface. Most ions are deflected/backscattered from their path as a result of collision with target atoms and some ions penetrate over a certain distance inside the sample. As a result of collisions, sample constituent atoms are displaced from their lattice positions. The collision also results in recoil and sputtering of constituent atoms, formation of defects, electron emission and excitation, photon emission, etc. (Melngailis 1987). Mixing of constituent atoms, phase transformation, crystallization, amorphization and permanent damage might also occur as a result of thermal- and radiation-induced effects. Ion implantation on target surface due to FIB operation and sputtering results in change of surface morphology and craters are formed as a result of atoms being removed. A schematic of focused ion–beam interaction with sample surface is shown in Fig. 1c. The collision of ions with target material nucleus and electrons can be considered separately due to large difference in their masses:

- Elastic or nuclear collision—between ion and nucleus. Kinetic energy and momentum are conserved. The incident ion recoils the target atom and scattering of ion takes place.
- Inelastic or electronic collision—between ion and electrons. It results in excitation and ionization of the constituent electrons.

Following main effects take place due to ion–solid interactions (Melngailis 1987):

- Thermal heating—The sample surface gets heated due to ion–beam interactions.
- Radiation damage—The sample is damaged due to displacement of atoms from their lattice positions. The depth of ion penetration depends on the ion beam energy, material properties and operating parameters such as incidence angle. The ions are implanted in the sample.
- Sputtering—The atoms are removed from sample surface due to incident ions. Sputtering occurs at low energies.
- Electron emission—The electrons are emitted from the target surface due to ion–solid interactions. These electrons are used for imaging.
- Chemical effects—These are produced due to ion–electron interaction and ion–atom interaction. Examples are ion-assisted etching, ion-induced deposition, etc.

The ion–solid interactions for amorphous materials can be modelled using Monte Carlo simulations by SRIM/TRIM (stopping and range of ions in matter, transport of ions in matter) codes developed by Ziegler and Biersack (1985). These simulations are helpful for calculation of sputter yield, interaction volume, etc. However, these calculations are based on binary collisions, and the effects of neighbouring atoms are not taken into account.

## *2.3 Focused Ion Beam Governing Parameters and Important Effects*

Focused ion beam nanofabrication is a complex process and requires accurate control of processing parameters for the desired fabrication. A brief introduction of important FIB governing parameters and their effects on milling are discussed in this section.

### 2.3.1 Acceleration Voltage

An extraction voltage is applied to pull the Ga ions from the wet tungsten needle tip. The energy and velocity of ions depend on the applied acceleration voltage in the ion column. Ions will travel faster if a higher acceleration voltage is applied, and thus, the energy imparted on the target sample will also be higher (Fu et al. 2000). An increase in the acceleration voltage does not influence the probe current. An acceleration voltage of 30 kV is generally used to get the highest possible resolution and sputtering yield (Orloff 1993). This value of acceleration voltage makes the system suitable for many applications like sputtering, implanting or imaging.

### 2.3.2 Beam Current

Ion beam current is an important parameter for fabrication of micro/nano-structures. It defines the resolution capability of FIB system. Beam spot size is controlled by the beam current. It is difficult to measure the spot size in practice; hence, the beam current is generally used as a process parameter. The sputtering yield is controlled by changing the beam current. At higher values of beam current (i.e. larger spot size), sputtering yield is high. The higher material removal rate is, however, at the expense of the fabrication accuracy. If a high-resolution and accurate profile is required, a low beam current must be used. During typical milling applications, a high beam current is used for bulk material removal applications, while low beam currents are used for fine polishing. The typical minimum spot size of Carl Zeiss Auriga system at MEMS department IIT Bombay is 8 nm at a beam current of 1 pA and acceleration voltage 30 kV.

### 2.3.3 Dwell Time

Dwell time in a FIB system is the duration of time for which the beam is stationary at a particular position (pixel). Ion beam dwell time defines the duration of time for which a particular pixel is scanned by the ion beam (Utke et al., 2008). The dwell time is generally of the order of microseconds (μs) to milliseconds (ms). Final geometry of FIB fabrication depends on the dwell time, making it an important parameter. There are two challenges associated with the optimization of the dwell time. First, excessively large dwell time results in redeposition of sputtered atoms/ions, and surface accuracy becomes poor. The fabrication depth is also more than the intended value. These effects are applicable for fabrication, where depth removed per pixel is of the order of beam diameter (Adams and Vasile 2006). Second, a very low dwell time results in undesired material removal outside the targeted area. This occurs in the fabrication of non-rectilinear profiles such as circle, ellipse, etc. A significant portion of target material is exposed to the unintended ion dose and results in an irregular profile and undesired milling (Adams and Vasile 2006). Thus, a careful choice and optimization of FIB dwell time is required for the desired accuracy of fabrication. This aspect is even more challenging for 3D features nanofabrication by FIB.

### 2.3.4 Ion Range

Focused ion beam with high-energy ions impacts the target surface. High-energy ions impart their energy to the surface atoms and travel a certain path inside the target material. The trajectory followed by the energetic ions is known as 'collision cascade', and the total length of the path travelled by ion is termed as 'range'. The projected values of ion range in amorphous targets can be calculated using the Monte Carlo simulation-based SRIM code developed by Ziegler and Biersack

**Table 1** The ion range and sputtering yield of various materials for 30 kV Gallium ions (Glass et al. 2008)

| Material | Si | Al | Cu | Ag |
|---|---|---|---|---|
| Ion range (nm) | 27 | 24 | 10 | 11 |
| Sputter yield (atoms/ion) | 2.6 | 4.4 | 11 | 14 |

(1985). The ion range depends on ion–solid interactions and material properties. Ion ranges of few different materials are as presented in Table 1.

### 2.3.5 Sputter Yield

Sputter yield is defined as the number of target atoms ejected per incident ion at the target surface. It depends on following parameters (Yao 2007):

- Incident ions—mass, energy, dose, incidence angle, etc.
- Target material—mass, crystal orientation, crystallinity, surface binding energies, conductivity, surface curvature, etc.

There exists a threshold value of the incident ion energy for each material, below which no sputtering takes place. Table 1 shows the sputter yield for four different materials with gallium as an ion source at 30 kV.

The milling time and sputter yield can be calculated as

$$\begin{aligned}\text{Sputter Rate} &= \left[\frac{\text{Volume Removed}}{\text{Ion Dosage}}\right] = \left[\frac{\text{Volume Removed}}{\text{Beam current} \times \text{Milling Time}}\right] \\ &= \left[\frac{\mathrm{d}x \times \mathrm{d}y \times \mathrm{d}z}{I_\mathrm{B} \times T}\right]\end{aligned} \tag{1}$$

$$\text{Milling Time} = \frac{\mathrm{d}x \times \mathrm{d}y \times \mathrm{d}z}{I_\mathrm{B} \times \text{Sputter Rate}} \tag{2}$$

$$\text{Sputter Yield} = \frac{\text{Number of atoms removed from the target surface}}{\text{Number of incindent ions}} \tag{3}$$

where $I_\mathrm{B}$ is the ion beam current used for milling, $T$ is the milling time and d$x$, d$y$, d$z$, are dimensions (length, width, depth) of the milled region.

### 2.3.6 Scan Mode and Pixel Spacing

The ion beam can be scanned over a target surface in two different modes—raster scan and serpentine scan (Yao 2007). In raster mode, scanning is done in the same direction. The beam always moves to initial point of next scanning line. Figure 2a shows the schematic diagram of FIB raster scanning. In this mode of scanning, the

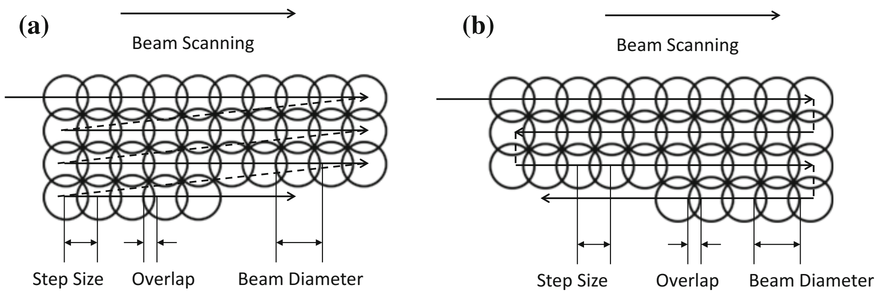


**Fig. 2** Schematic illustration of FIB scanning: **a** raster scan and **b** serpentine scan

sputtered atoms continuously redeposit on the milling area. It results in loss of fabrication accuracy. Raster scanning is suitable for fabrication of V-shaped channels or inclined bottom surfaces. In serpentine scanning, ion beam moves in reverse directions for next scan line. It results in faster operation and fabrication time is less as compared to raster scan for the same area. Schematic diagram representing serpentine scanning mode is shown in Fig. 2b. The redeposition of sputtered material is less in serpentine scanning mode, as the redeposited atoms from the previously scanned line are removed in the subsequent line scan. This mode of scanning is favourable for high aspect ratio structures with vertical side-walls and flat bottom. Pixel spacing can be defined as the distance between the centres of two adjacent pixels. Milling by FIB will be uniform, if the spacing between adjacent pixels and scan lines is proper and small enough (Tseng 2005).

### 2.3.7 Beam Overlap

The scanning in FIB process, as illustrated in the previous section, takes place along a predefined path and ion beam is moved to subsequent pixel locations with a distance equal to step size. Focused ion beam is blanked while moving from one pixel to another. The ion beam diameter and step size, in addition to dwell time, are two important parameters that determine the profile of depth being milled. Beam overlap is defined with respect to step size (Yao 2007)

$$\text{Beam Overlap} = \frac{\text{Beam Diameter} - \text{Step Size}}{\text{Beam Diameter}} \quad (4)$$

The concept of beam overlap is represented schematically in Fig. 3. Beam overlap is 50%, if the step size is half of the beam diameter. It is a critical FIB parameter and must be optimized for different applications. Negative overlap for deposition, zero overlap for etching and positive overlap are generally used for milling applications.

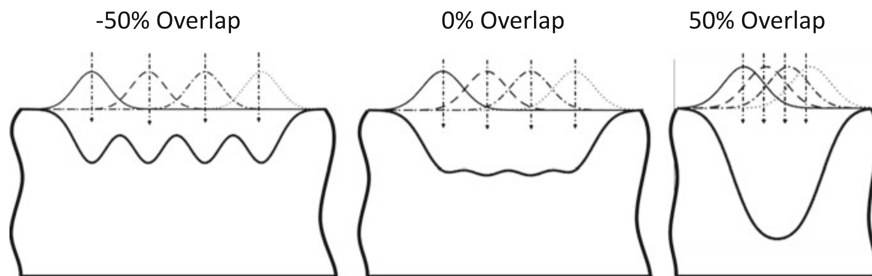


**Fig. 3** Concept of beam overlap in FIB and effect on fabrication profile: negative, zero and positive overlap

## *2.4 Focused Ion Beam—Process Capabilities*

### 2.4.1 Focused Ion Beam Imaging

In FIB imaging, similar to a scanning electron microscope, the beam is scanned over the sample surface. The secondary ions and electrons are generated due to the interaction between incident ions and surface atoms. These secondary ions or electrons are collected for the purpose of imaging by means of biased detectors. The detectors collect emitted ions or electrons based on the voltage applied to it. The resolution of FIB imaging depends upon the ion beam spot size (Reyntjens and Puers 2001).

Focused ion beam is proved to be a powerful tool for material analysis and characterization. The channelling contrast produced by FIB is better than the contrast provided by the electrons in an SEM. This capability is utilized for observing grain boundary orientations and crystal defects such as dislocations. However, due to ion–beam interactions with the sample surface, some damage also occurs. It limits the use of FIB for imaging of soft materials. Some of the ions from the beam penetrate into the sample and get implanted in the surface, resulting in change of surface properties. The depth of implantation depends upon the beam energy, and material damage up to an extent takes place based on the beam parameters. These effects can be reduced by using a low energy and finely focused beam of ions.

### 2.4.2 Focused Ion Beam Milling

Material from the sample surface can be removed precisely using a high energy and finely focused beam of ions. If the high energy beam is scanned over the surface, it results in sputtering of atoms from the sample surface. The milling process can be observed in situ and sample surface can be analysed by FIB/SEM imaging. The milling rate by FIB is generally small, as the material removal takes place atom by

atom, and usually the sputtering is accompanied by redeposition of the sputtered atoms from the surface. To enhance the milling rate, an etching gas can be used in work chamber. This technique is called 'gas-assisted etching (GAE)' (Reyntjens and Puers 2001). Gas-assisted FIB etching can be regarded as a local version of plasma etching or reactive ion etching with much higher ion energy (Utke et al. 2008). Following steps are followed in gas-assisted FIB-induced etching (Yao 2007):

- A chemically neutral reactive gas through a nozzle is adsorbed on the sample surface.
- The gas reacts with the sample either in the presence or absence of ion beam.
- Volatile products are formed (desorption), which are removed from vacuum.

Ion implantation, redeposition, etc. can be reduced using gas-assisted ion beam etching. However, care must be taken to avoid any spontaneous reaction of the etching gas with the target surface.

### 2.4.3 Focused Ion Beam Deposition

Focused ion beam can be used for deposition of metal and insulator materials (Reyntjens and Puers 2001). The operating principle is analogous to chemical vapour deposition (CVD). Generally, deposition of platinum and tungsten is done on commercially available instruments. There are various phenomena that occur when an ion beam is scanned over target surface, where precursor gas molecules are previously desorbed:

- Desorption of the molecules,
- Dissociation of the molecules and
- Reaction of molecules with target material.

A deposition layer is sprayed over sample surface in the form of a gas. The ion beam is subsequently scanned over the sample surface and the sprayed gas is decomposed by the action of an ion beam. The desired reaction products remain on the surface as a thin film, while the volatile products are removed with the help of vacuum inside the chamber. The deposited material is not completely pure, as some organic contaminants, as well as gallium ions, are also implanted in the deposits. Tungsten, platinum, carbon, etc. are some of the common materials that can be deposited by FIB.

There are many similarities between FIB-induced deposition and etching process. Deposition and etching gases both can adsorb/desorb without reacting with the sample surface. However, some etching gases (for example, chlorine on silicon) are also able to react with the sample surface. For etching, sputtering due to FIB will add to the material removal. While in case of deposition, sputtering will complete the process. The basic requirements for precursor gas are same for both deposition and etching. The gas should stick to the surface for activation/dissociation for etching/deposition (Yao 2007).

### 2.5 Focused Ion Beam Limitations

Main issues/limitations in FIB milling for 3D micro/nanofabrication are as follows (Fu et al. 2000; Lehrer et al. 2001):

- *Overlap effect*—To fabricate a smooth surface, the spacing between the pixels should be less than the beam size. However, this results in more milling than intended and consequently depth milled is higher.
- *Beam tail effect*—This effect is due to the beam profile, which is generally Gaussian distribution. The tail of the beam results in undesired milling, thus making it difficult to control the depth and maintain the geometric accuracy.
- *Sputter yield*—In addition to other beam parameters, the sputter yield also depends on the angle of incidence of the ion beam. As the machining progresses, the surface geometry is changed, which in turn changes the effective angle at which the ion beam hitting the surface. Thus, the sputter yield changes with time, leading to the non-uniform material removal at different regions of the geometry.
- *Redeposition effect*—Based on the amount of materials removed and aspect ratio of the target geometry, some of the sputtered atoms redeposit on the sample surface itself, which results in fabrication inaccuracies.

In addition to the above-mentioned limitations, FIB also has scalability limitations. This makes FIB milling restricted to a smaller volume for material characterisation/removal applications; however, this issue is now being addressed by employing Xe-based plasma FIB (Burnett et al. 2016).

## 3 The Optimization Model

Focused ion beam process planning is important for fabrication of desired structures from accuracy point of view. Focused ion beam is a complex process and involves material interaction of ion beam during the process. An optimization model from the literature (Qin et al. 2013) is adapted here to optimize the dwell time for maintaining accuracy and fabrication of desired profile using FIB milling.

### 3.1 Scanning for FIB Milling

A charged beam of ions is scanned over the target substrate for machining in FIB milling. The substrate is divided into a grid of pixels for beam control and machining accuracy. The machining depth depends upon the dwell time, i.e. the time for which a particular pixel is scanned by FIB. However, when the beam is scanned over a certain pixel (say $(x_j, y_j)$), it results in milling at nearby pixel (say

$(x_i, y_i)$) due to the Gaussian distribution of beam. The effect of nearby pixels being milled due to FIB scanning at certain pixels is shown in Fig. 4. It is also clear from Fig. 4, if a particular pixel is scanned for a longer duration (more dwell time), it will result in more depth being milled. Thus, fabrication profile can be varied by controlling the dwell time. The standard Gaussian normal distribution is given by

$$G(x) = \frac{1}{\sqrt{2\pi\sigma^2}}\left[e^{-\frac{(x-\mu)}{2\sigma^2}}\right] \tag{5}$$

where $\sigma$ is the standard deviation of the beam. The total depth being machined due to FIB milling can be written as

$$z_i = \sum_{j=1}^{M} Y_s t_j \left[e^{-\frac{\left[(x_i-x_j)^2+(y_i-y_j)^2\right]}{2\sigma^2}}\right] \tag{6}$$

where $M$ is the number of pixels to be machined, $z_i$ is the machined depth at $i$th pixel, $Y_s$ is the erosion rate and $t_j$ is the dwell time (which is decision variable) at $j$th pixel. The above equation can be written as

$$z_i = \sum_{j=1}^{M} a_{ij} t_j = \boldsymbol{A_i t}, \quad \text{for } i = 1, 2, \ldots N \tag{7}$$

where $N$ is the total number of pixels on substrate, $a_{ij}$ is the milling coefficient and $\boldsymbol{A}$ is an $N \times M$ matrix to measure the milling coefficients.

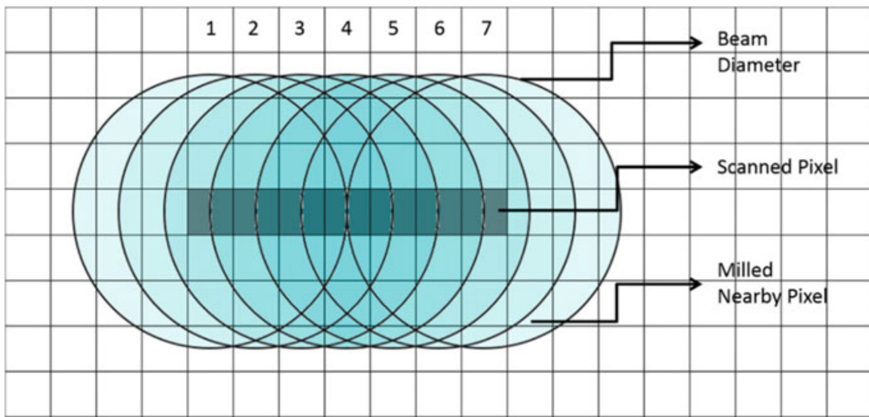


**Fig. 4** Effect of beam shape and dwell time on fabrication depth at different pixels—colour intensity represents the fabrication depth

### 3.2 The Objective Function

The decision variable dwell time $\boldsymbol{t}$ should be optimized such that it results in material removal $\boldsymbol{At}$ (i.e. fabricated profile) close to the desired geometry profile $z^{o}$. A quadratic optimization problem is set up to minimize the error between $\boldsymbol{At}$ and $z^{o}$ in the following form:

$$\begin{aligned} &\text{minimize } F(\boldsymbol{t}) = \|\boldsymbol{At} - \boldsymbol{z^o}\|_2^2 \\ &\text{subject to, } \boldsymbol{t} \geq 0 \end{aligned} \tag{8}$$

The objective function in $F(\mathbf{t})$ is rewritten in the following form to represent the following standard quadratic programming problem:

$$\begin{aligned} &\text{minimize } F(\boldsymbol{t}) = \boldsymbol{t}^T\boldsymbol{Qt} + 2\boldsymbol{p}^T\boldsymbol{t} + r \\ &\text{subject to, } \boldsymbol{t} \geq 0 \end{aligned} \tag{9}$$

where

$$\begin{aligned} \boldsymbol{Q} &= \boldsymbol{A}^T\boldsymbol{A}, \\ \boldsymbol{p} &= -\boldsymbol{A}^T\boldsymbol{z^o} \\ r &= (\boldsymbol{z^o})^T\boldsymbol{z^o} \end{aligned} \tag{10}$$

### 3.3 Solution

A multiplicative updates algorithm from the literature (Yang and Laaksonen 2007) is used for solution of the above non-negative quadratic programming problem. If $\boldsymbol{t}^0$ is an initial value of dwell time $\boldsymbol{t}$, and $\boldsymbol{t}^k$ ($k > 0$) is the value from the $k$th update, algorithm can be written as

$$t_j^{k+1} \leftarrow \frac{\max\left[-p_j, 0\right]}{(\boldsymbol{Qt}^k)_j} t_j^k \tag{11}$$

## 4 Simulation Results

The optimization algorithm from the previous section is used to simulate a spherical cavity using MATLAB. The beam current is taken as 20 pA, $X = Y = 600$ nm, and the pixel size is 3 nm. Results are shown in Fig. 5 on a 200 × 200 grid (since pixel size is 3 nm). The beam diameter at this current is 17 nm (Zeiss Auriga dual beam

FIB-SEM system), and step size is taken as 3 nm. The plot in Fig. 5a is the desired spherical shape with $z^{o}$ = 60 nm. Figure 5b shows the simulation results obtained by FIB scanning. The difference between $\boldsymbol{At}$ (simulated geometry) and $z^{o}$ (desired geometry), i.e. error is shown in Fig. 5c. It can be seen from the figure that the error is significant only at the boundaries. This is because no actual machining takes place at boundary pixels, and the depth obtained is only because of the milling at nearby pixels. Thus, the optimization model is capable of producing accurate results. Several other simulations have also been run using the optimization model for different profiles, in order to check the validity of the optimization algorithm, and no significant error was observed between desired and simulated profile.

Further, optimization of dwell time for desired and accurate 3D optical elements by FIB can be obtained using the developed algorithm. Fabrication of 3D optical elements such as lenses on optical fibre for waveguide coupling (Schiappelli et al. 2004; Melkonyan et al. 2017), Fresnel zone plates (FZPs) for X-rays focusing, etc. forms an important field of study due to the unique capability of these elements. Fresnel zone plates are very popular optical components for applications in X-ray microscopy (Quiney et al. 2006) with the capability of focusing X-rays. X-rays can have a high penetration depths and resolution, allowing the use of X-rays for

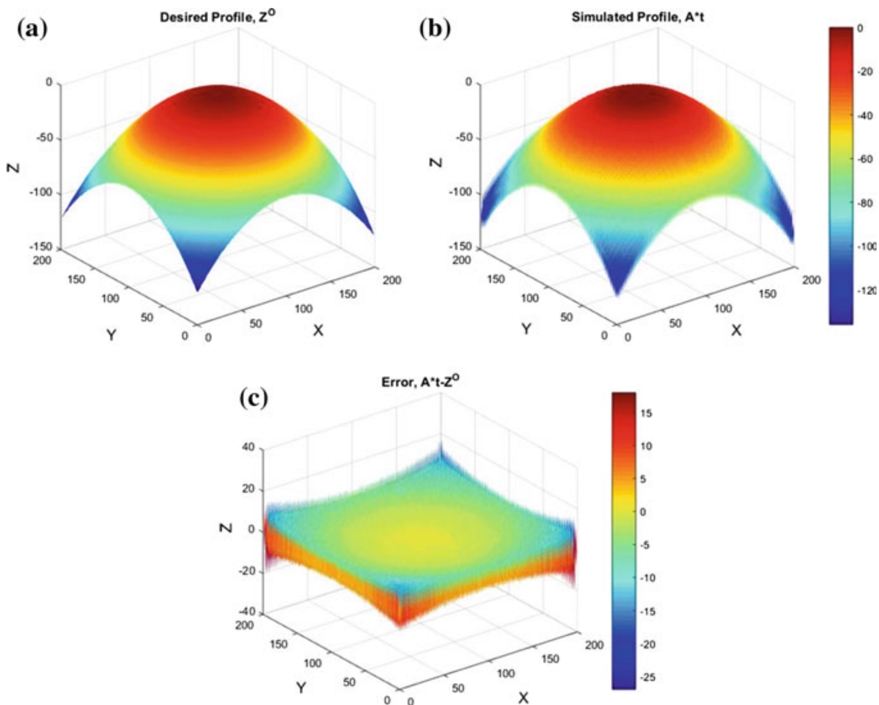


**Fig. 5** Simulation results for a spherical profile obtained from optimization algorithm at a beam current of 20 pA and pixel size of 3 nm: **a** desired spherical profile, **b** simulated spherical profile and **c** error between the desired and simulated profile

material characterization applications (Attwood 1999). As a result, FZPs become important optical elements for applications in microscopic imaging and nanotechnology. Researchers all over the world have presented a variety of FIB fabrication methods for FZPs (Keskinbora et al. 2013a, b; Vijayakumar et al. 2014; Vijayakumar and Bhattacharya 2015; Sanli et al. 2015; Rodrigues Ribeiro et al. 2016). Experimental demonstrations of FZPs (Mote et al. 2010) as well as sub-wavelength focusing technique using metallic coatings also exist (Mote et al. 2008). However, there is still a need to explore this method for better control and improvement of fabrication accuracy. Here, we design and optimize FZP fabrication by FIB using the developed optimization algorithm as an example.

FZPs are diffractive optical elements and these are made of alternate opaque and transparent zones. The FZPs are designed according to

$$r_n = \sqrt{n\lambda f + n^2\lambda^2/4} \tag{12}$$

where $r_n$ is the radius of $n$th zone, $\lambda$ is the wavelength and $f$ is the focal distance (Attwood 1999). The resolution of FZP depends on the outermost zone and is given by

$$\Delta r_{\text{Rayleigh}} = 1.22\Delta r \tag{13}$$

where $\Delta r_{\text{Rayleigh}}$ is the Rayleigh resolution limit and $\Delta r$ is the width of outermost FZP zone (Attwood 1999).

Figure 6 show the simulation results for FZP. The simulation results shown here are for a binary FZP of diameter 100 µm, focal length of 150 µm and for a wavelength of 660 nm. The beam current for the simulation is taken as 500 pA, $X = Y = 100$ µm, and a large value of pixel size 200 nm is chosen. Results are shown in Fig. 6 on a 500 × 500 grid (since pixel size is 200 nm). The beam diameter at this current is 50 nm for Zeiss Auriga dual beam FIB-SEM system. The reason for selecting large pixel size for FZP simulation is to reduce the simulation time maintaining accuracy, as the size of FZP is large (100 µm). The results from Fig. 6c indicate a very small value of error. It is due to the binary nature of simulated FZP, as it did not involve any curved features. Next, an attempt is made to validate the optimization results with experiments.

## 5 Results of Focused Ion Beam Fabrication

Experiments have been carried out on Zeiss Auriga dual beam FIB-SEM system using Ga ion beam. This system allows smallest spot size of 8 nm at a beam current of 1 pA. It allows milling, deposition and imaging using ion and electron beam. Focused ion beam milling is a very powerful tool and it enables micro/nano-fabrication with great accuracy. Simulation profile of FZP in the previous section is fabricated using FIB milling for demonstration. The system allows

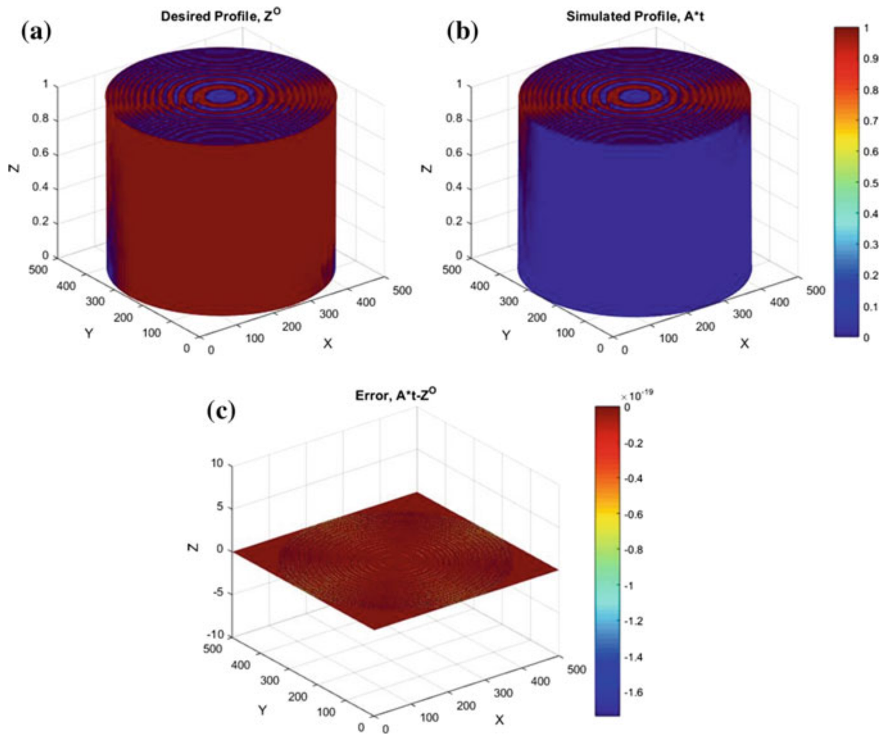


**Fig. 6** Simulation results for fabrication of Fresnel zone plate obtained from optimization algorithm at a beam current of 500 pA and pixel size of 200 nm: **a** desired profile, **b** simulated profile and **c** error between the desired and simulated profile

feature-based milling, and bitmap images consisting of designed pattern can be milled by choosing desired beam current, dwell time, acceleration voltage, etc. A bitmap image consisting of ring patterns based on the FZP design is created using MATLAB. Figure 7a shows the bitmap image used for a binary FZP of diameter 100 μm, focal length of 150 μm for a wavelength of 660 nm. This bitmap image has been used on FIB-SEM system for fabrication on silicon. Focused ion beam is scanned over the black areas in the bitmap image, and milling takes place at these areas only. Scanning electron microscopic image of FZP fabricated on silicon using FIB milling is shown in Fig. 7b. The fabrication has been done using Gallium ion beam at a beam current of 500 pA and acceleration voltage of 30 kV. Next, atomic force microscopic (AFM) characterization of fabricated FZP is done. Only a portion of FZP is scanned due to the scanning limitations of AFM. Figure 8 shows the AFM characterization results of fabricated FZP. 2D and 3D profiles of FIB fabricated FZP in Fig. 8a, b, respectively, demonstrate the fine accuracy and capability of the process. Figure 8c represents the surface profile of fabricated FZP.

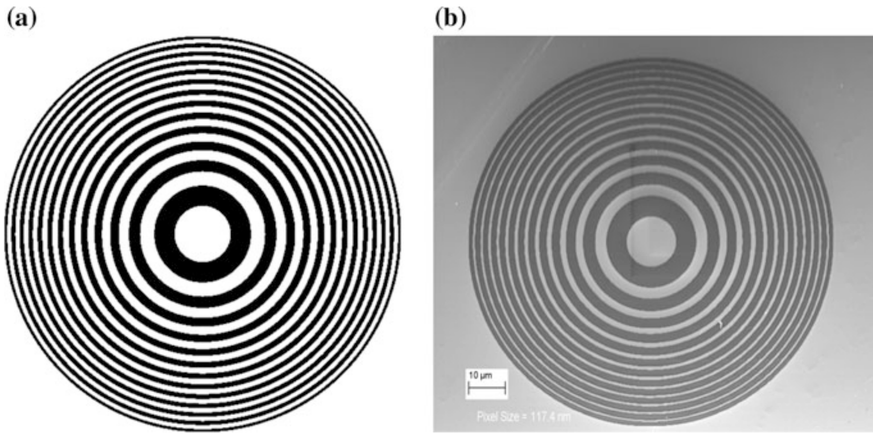


**Fig. 7** Binary Fresnel zone plate fabrication by focused ion beam milling: **a** bitmap image used in the Zeiss Auriga dual beam FIB-SEM system, and **b** scanning electron microscopic image of fabricated FZP

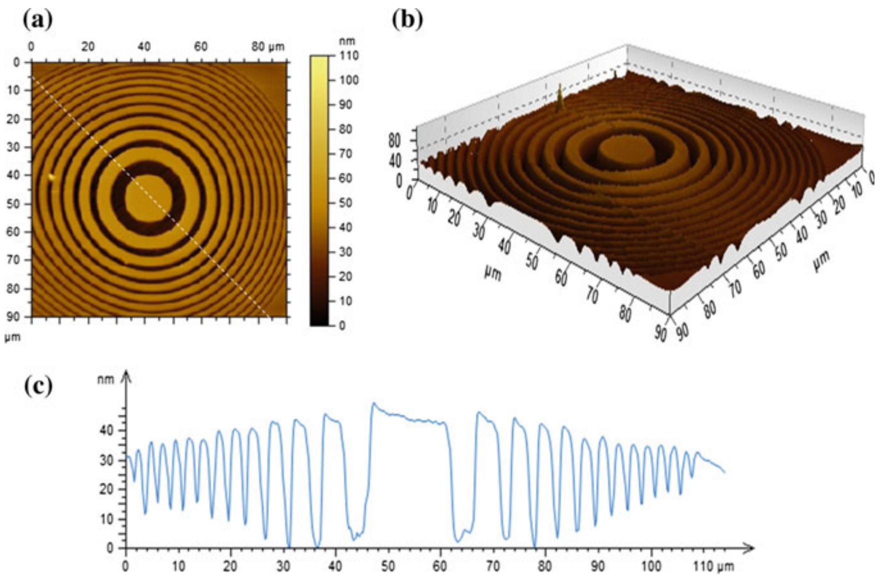


**Fig. 8** Atomic force microscopic (AFM) results of focused ion beam milled Fresnel zone plate: **a** 2D AFM image, **b** 3D AFM image and **c** variation of surface profile along white line indicated in (**a**)

## 6 Conclusions

This work presented focused ion beam milling process development and optimization for fabrication of optical applications. An optimization model has been developed and used to simulate the FIB milling process for fabrication of desired profiles. Ion beam dwell time is an important parameter for the accurate fabrication. Beam dwell time is optimized for the required accuracy and an example has been presented for a spherical profile. Simulation results have been shown to predict the fabrication geometry fairly well. The amount of error between the desired geometry and the simulated geometry is quite low, indicating good results and validity of the optimization algorithm. Further, simulation results for optimization of FZP fabrication are presented, which have been able to predict the required fabrication geometry well at the given beam parameters. The error between the desired geometry and simulated FZP geometry is insignificant (<0.1%) due to its binary nature. The FZP structure is fabricated using FIB process on silicon and characterized using AFM. This approach can be further extended to fabrication of 3D optical elements and complex micro/nano-structures by FIB milling. To summarize,

- A framework for optimal solution of FIB dwell time through an iterative approach.
- Dwell time was optimized by formulation and solution of a quadratic programming problem, minimizing the error between desired and simulated geometry. Simulation examples were demonstrated for a spherical profile and FZP. Experiments were carried out for fabrication of a binary FZP by FIB.
- The approach can be extended further for FIB fabrication of 3D nanostructures and optical elements maintaining high accuracy.

**Acknowledgements** The authors acknowledge the financial support by IRCC, IIT Bombay via Seed Grant: Spons/ME/I14079-1/2014. The first author acknowledges the Ph.D. scholarship support by IITB Monash Research Academy.

## References

Adams, D.P., and M.J. Vasile. 2006. Accurate focused ion beam sculpting of silicon using a variable pixel dwell time approach. *Journal of Vacuum Science and Technology B* 24: 836–844.

Adineh, V.R., B. Liu, R. Rajan, W. Yan, and J. Fu. 2015. Multidimensional characterisation of biomechanical structures by combining atomic force microscopy and focused ion beam: A study of the rat whisker. *Acta Biomaterialia* 21: 132–141.

Al-Abboodi, A., J. Fu, P.M. Doran, and P.P.Y. Chan. 2013. Three-dimensional nanocharacterization of porous hydrogel with ion and electron beams. *Biotechnology and Bioengineering* 110: 318–326.

Attwood, D. 1999. *Soft X-rays and extreme ultraviolet radiation, soft X-rays and extreme ultraviolet radiation: Principles and applications*. Cambridge University Press.

Burnett, T.L., R. Kelley, B. Winiarski, L. Contreras, M. Daly, A. Gholinia, M.G. Burke, and P. J. Withers. 2016. Large volume serial section tomography by Xe Plasma FIB dual beam microscopy. *Ultramicroscopy* 161: 119–129.

Fu, J., and S. Joshi. 2010. Optimization based geometric modeling of nano/micro scale ion milling of organic materials for multidimensional bioimaging. *Journal of Nanotechnology in Engineering and Medicine* 1: 031003.

Fu, Y.Q., N.K.A. Bryan, O.N. Shing, and N.P. Hung. 2000. Influence of the redeposition effect for focused ion beam 3D micromachining in silicon. *International Journal of Advanced Manufacturing Technology* 16: 877–880.

Glass, G.A., J.F. Dias, A.D. Dymnikov, and B. Rout. 2008. 900 keV gold ion sputter etching of silicon and metals. *Nuclear Instruments and Methods in Physics Research Section B: Beam Interactions with Materials and Atoms* 266: 3330–3331.

Keskinbora, K., C. Grévent, M. Bechtel, M. Weigand, E. Goering, A. Nadzeyka, L. Peto, S. Rehbein, G. Schneider, R. Follath, J. Vila-Comamala, H. Yan, and G. Schütz. 2013a. Ion beam lithography for Fresnel zone plates in X-ray microscopy. *Optics Express* 21: 11747–11756.

Keskinbora, K., C. Grévent, and U. Eigenthaler. 2013b. Rapid prototyping of Fresnel zone plates via direct $Ga^+$ ion beam lithography for high-resolution X-ray imaging. *ACS Nano* 7: 9788–9797.

Kim, C.S., S.H. Ahn, and D.Y. Jang. 2012. Review: Developments in micro/nanoscale fabrication by focused ion beams. *Vacuum* 86: 1014–1035.

Lehrer, C., L. Frey, S. Petersen, and H. Ryssel. 2001. Limitations of focused ion beam nanomachining. *Journal of Vacuum Science & Technology B: Microelectronics and Nanometer Structures Processing, Measurement, and Phenomena* 19: 2533.

Melkonyan, H., K. Sloyan, K. Twayana, P. Moreira, and M. Dahlem. 2017. Efficient fiber-to-waveguide edge coupling using an optical fiber axicon lens fabricated by focused ion beam. *IEEE Photonics Journal* 9: 1–9.

Melngailis, J. 1987. Focused ion beam technology and applications. *Journal of Vacuum Science and Technology B* 5: 469–495.

Mote, R.G., and L. Xiaomin. 2017. *Focused ion beam (FIB) nanofinishing for ultra-thin TEM sample preparation*, 155–176. Nanofinishing science and technology, micro and nanomanufacturing series. CRC Press.

Mote, R.G., S.F. Yu, B.K. Ng, W. Zhou, and S.P. Lau. 2008. Near-field focusing properties of zone plates in visible regime–new insights. *Optics Express* 16: 9554–9564.

Mote, R.G., S.F. Yu, A. Kumar, W. Zhou, and X.F. Li. 2010. Experimental demonstration of near-field focusing of a phase micro-Fresnel zone plate (FZP) under linearly polarized illumination. *Applied Physics B* 102: 95–100.

Orloff, J. 1993. High-resolution focused ion beams. *Review of Scientific Instruments* 64: 1105–1130.

Qin, R., J. Fu, Z. Yin, and C. Zheng. 2013. Large-scale process optimization for focused ion beam 3-D nanofabrication. *International Journal of Advanced Manufacturing Technology* 64: 587–600.

Quiney, H.M., A.G. Peele, Z. Cai, D. Paterson, and K.A. Nugent. 2006. Diffractive imaging of highly focused X-ray fields. *Nature Physics* 2: 101–104.

Reyntjens, S., and R. Puers. 2001. A review of focused ion beam applications in microsystem technology. *Journal of Micromechanics and Microengineering* 11: 287–300.

Rodrigues Ribeiro, R.S., P. Dahal, A. Guerreiro, P.A.S. Jorge, and J. Viegas. 2016. Compact solutions for optical fiber tweezers using Fresnel zone and phase lenses fabricated using FIB milling. In *Proceedings of SPIE.*

Sanli, U.T., K. Keskinbora, K. Gregorczyk, J. Leister, N. Teeny, C. Grévent, M. Knez, and G. Schütz. 2015. High-resolution high-efficiency multilayer Fresnel zone plates for soft and hard x-rays. In: *Proceedings of SPIE.*

Schiappelli, F., R. Kumar, M. Prasciolu, D. Cojoc, S. Cabrini, M. De Vittorio, G. Visimberga, A. Gerardino, V. Degiorgio, and E. Di Fabrizio. 2004. Efficient fiber-to-waveguide coupling by a lens on the end of the optical fiber fabricated by focused ion beam milling. *Microelectronic Engineering, Micro and Nano Engineering* 73: 397–404.

Tseng, A.A. 2005. Recent developments in nanofabrication using focused ion beams. *Small* 1: 924–939.

Utke, I., P. Hoffmann, and J. Melngailis. 2008. Gas-assisted focused electron beam and ion beam processing and fabrication. *Journal of Vacuum Science and Technology B* 26: 1197–1276.

Vijayakumar, A., and S. Bhattacharya. 2015. Design of multifunctional diffractive optical elements. *Optical Engineering* 54: 24104.

Vijayakumar, A., U. Eigenthaler, K. Keskinbora, G.M. Sridharan, V. Pramitha, M. Hirscher, J. P. Spatz, and S. Bhattacharya. 2014. Optimizing the fabrication of diffractive optical elements using a focused ion beam system. *Micro-Optics* 2014 (9130): 1–8.

Yang, Z., and J. Laaksonen. 2007. Multiplicative updates for non-negative projections. *Neurocomputing* 71: 363–373.

Yao, N. 2007. *Focused ion beam systems: Basics and applications*. Cambridge University Press.

Ziegler, J.F., and J.P. Biersack. 1985. The stopping and range of ions in matter. In *Treatise on heavy-ion science*, ed. D.A. Bromley, 93–129. US: Springer.